

Convective Precipitation Nowcasting Using U-Net Model

Lei Han[✉], Member, IEEE, He Liang, Haonan Chen[✉], Senior Member, IEEE,
Wei Zhang[✉], Member, IEEE, and Yurong Ge

Abstract—Convective precipitation nowcasting remains challenging due to the fast change in convective weather. Radar images are the most important data source in nowcasting research area. This study proposes a radar data-based U-Net model for precipitation nowcasting. The nowcasting problem is first transformed into an image-to-image translation problem in deep learning under the U-Net architecture, which is based on convolutional neural networks (CNNs). The input of the model is five consecutive radar images; the output is the predicted radar reflectivity image. The model consists of three operations: upsampling, downsampling, and skip connection. Three methods, U-Net, TREC, and TrajGRU, are used for comparison in the experiments. The experimental results show that both deep learning methods outperform the TREC method, and the CNN-based U-Net can achieve almost the same performance as TrajGRU which is a recurrent neural network (RNN)-based model. With the advantages that U-Net is simple, efficient, easy to understand, and customize, this result shows the great potential of CNN-based models in addressing time-series applications.

Index Terms—Deep learning, precipitation nowcasting, U-Net, weather radar.

I. INTRODUCTION

CONVECTIVE precipitation nowcasting plays an important role in operational weather forecast service, but it remains challenging due to the small spatial scale and short lifetime of convective weather. Weather radar is the only observational instrument which can provide 3-D reflectivity data with high spatial-temporal resolution.

Traditional convective precipitation nowcasting methods mainly depend on radar image extrapolation which can be roughly classified into two categories: cross correlation methods and centroid tracking methods [1]–[3]. The cross correlation methods are essentially optical flow methods which use the 2-D radar reflectivity images to compute the optical flow or motion vector field to forecast the storm movement.

Manuscript received April 21, 2021; revised June 26, 2021; accepted July 26, 2021. This work was supported in part by the National Key Research and Development Program of China under Grant 2018YFC1507504 and in part by the National Natural Science Foundation of China under Grant 41875049. The work of Haonan Chen was supported by Colorado State University. (*Corresponding author: Wei Zhang*.)

Lei Han, He Liang, Wei Zhang, and Yurong Ge are with the College of Information Science and Engineering, Ocean University of China, Qingdao 266100, China (e-mail: hanlei@ouc.edu.cn; lianghe@stu.ouc.edu.cn; weizhang@ouc.edu.cn; yurongge@ouc.edu.cn).

Haonan Chen is with the Department of Electrical and Computer Engineering, Colorado State University, Fort Collins, CO 80523 USA (e-mail: haonan.chen@colostate.edu).

Digital Object Identifier 10.1109/TGRS.2021.3100847

The centroid-type methods first detect isolated storm cells at current time and try to associate storms across two consecutive time steps, and then forecast the storm movement using the centroid of identified storm. The main advantage of the centroid-type method is that it can give physical data of each storm such as storm area, top, or volume. The main advantage of the cross correlation method is that it can give a radar reflectivity image as the forecast which is welcome by operational forecasters.

In recent years, deep learning has gained breakthroughs in image classification [4]–[7], image segmentation [8]–[10], and other various fields [11]–[14]. Some researchers have applied it to nowcasting area [15]–[20], and most of the existing deep learning nowcasting methods are based on recurrent neural network (RNN). Shi *et al.* [15] first proposed an RNN-based model, the convolutional long short-term memory (ConvLSTM), to capture the spatial and temporal features of radar echo sequence. They considered precipitation nowcasting as a spatiotemporal sequence prediction problem. Different from ConvLSTM which replaces all full connections in the LSTM cell with convolutions, Shi *et al.* [16] improved the nowcasting model using the trajectory gated recurrent units (TrajGRUs) which carries out trajectory convolution between different time steps to effectively learn the structure of spatial variations for recurrent connections. Also inspired by ConvLSTM, Wang *et al.* [17] proposed a predictive recurrent neural network (PredRNN) which used a unified memory pool memorizing both temporal variations and spatial appearances. In this model, spatial and temporal information is conveyed vertically through the layers of stacked RNNs and horizontally through the states of all RNNs. Furthermore, Wang *et al.* [18] proposed the PredRNN++ method which uses causal LSTM and a gradient highway unit. It can strengthen the internal forward information flow through causal LSTM and the backward gradient through gradient highway. Overall, the RNN-based nowcasting models have complicated structure which requires more experience and computational resources to optimize. In addition, they require memory-bandwidth-bound computation which often limits their applications [21].

In short, all the above models are RNN-based model which is considered good at sequence learning. Relatively, convolutional neural network (CNN) is considered good at spatial learning and relatively less used in sequence learning [22]. A typical successful CNN model is U-Net, which was proposed first in image segmentation field [10]. U-Net is

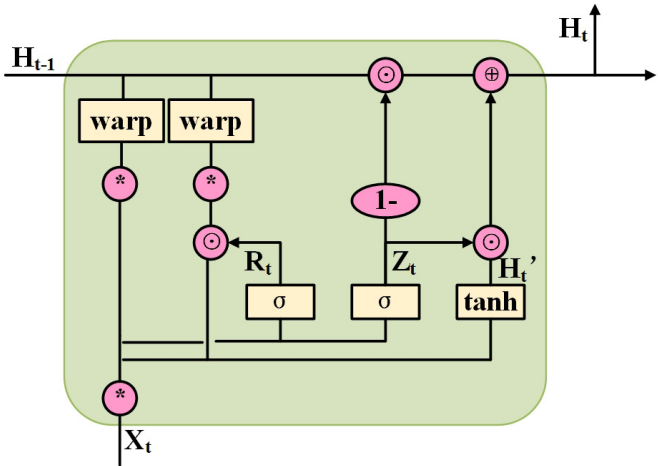


Fig. 1. Structure of TrajGRU neuron, which uses the warp operation to perform location-dependent dynamic convolution. The detailed information is given in Section II.

constructed by stacking downsampling convolutional modules on the left side and upsampling convolutional modules on the right side yielding a unique U-shape network architecture. Considering its flexibility and easy to extend to different applications, its framework is further explored in this study. This study presents a CNN-based U-Net model for convective precipitation nowcasting.

This article is organized as follows. Section II briefly introduces some related work about precipitation nowcasting. Section III describes the dataset used in this article. Section IV describes the detailed architecture of the model. Section V shows the evaluation results. The main results of this study are concluded in the last section.

II. RELATED WORK

A typical cross correlation method is the tracking radar echoes by correlation (TREC) which is the first widely used operational method in nowcasting area [23]. It divides a radar image into many small patches first, and then calculates the coefficients between patches at two consecutive radar images. Two matched patches can decide a motion vector for each grid point. Finally, these motion vectors can be used for prediction.

TrajGRU is a sequence deep learning method, which is an extension of the convolutional LSTM/GRU [15]. Contrary to convLSTM/GRU, the recurrent connections of TrajGRU are responsible for dynamically determining the location-dependent spatiotemporal patterns. TrajGRU generates a flow field from the current input and previous hidden states, and then warps previous hidden states through bilinear sampling (see Fig. 1). The output of the TrajGRU neuron H_t is given as follows:

$$U_t, V_t = \gamma(X_t, H_{t-1}) \quad (1a)$$

$$Z_t = \sigma \left(W_{xz} * X_t + \sum_{l=1}^L W_{hz}^l * \text{warp}(H_{t-1}, U_{t,l}, V_{t,l}) \right) \quad (1b)$$

$$R_t = \sigma \left(W_{xr} * X_t + \sum_{l=1}^L W_{hr}^l * \text{warp}(H_{t-1}, U_{t,l}, V_{t,l}) \right) \quad (1c)$$

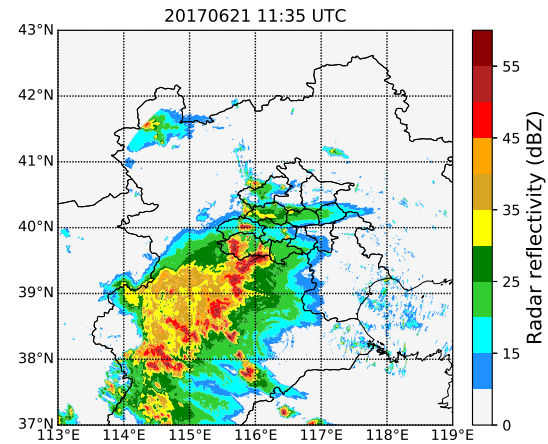


Fig. 2. Selected study domain in this article. The color map stands for radar composite reflectivity.

$$H'_t = f \left(W_{xh} * X_t + R_t \odot \left(\sum_{l=1}^L W_{hh}^l * \text{warp}(H_{t-1}, U_{t,l}, V_{t,l}) \right) \right) \quad (1d)$$

$$H_t = (1 - Z_t) \odot H'_t + Z_t \odot H_{t-1}. \quad (1e)$$

Here, L is the total number of allowed links. $U_t, V_t \in \mathbb{R}^{L \times H \times W}$ are the flow fields learned by a structure network γ . R_t and Z_t are the reset and update gates of the GRU cell, respectively. W_{hz}^l , W_{hr}^l , and W_{hh}^l are the weights. The $\text{warp}(H_{t-1}, U_{t,l}, V_{t,l})$ function is responsible to dynamically determine the recurrent connections.

The input of TrajGRU is five past consecutive radar images and the output is predicted radar images. The experimental results in [16] show that TrajGRU is superior to traditional cross correlation methods and convolutional LSTM/GRU in capturing the spatiotemporal correlations.

Han *et al.* [24] propose a CNN method to nowcast convective storms. They divide the study domain into many position-fixed small boxes and turn the nowcasting problem into a classification problem, i.e., will a radar echo greater than 35 dBZ appear in a box at the forecast time? The difference between this CNN method and the proposed U-Net method is that it uses typical CNN structure compared with the U-shape structure of U-Net. The CNN output is classification results, whereas the U-Net method output is radar reflectivity images.

III. DATA

In this study, radar reflectivity mosaic images are used as the dataset. All radar images are provided by the Beijing Meteorological Service (BMS) in China. The 3-D mosaic with a spatial resolution of 1 km and temporal resolution of 6 min is produced using six operational radars in northern China, including four S-band radars (located in Shijiazhuang, Beijing, Qinhuangdao, and Tianjin) and two C-band radars (located in Zhangbei and Chengde) from the network of the China Next Generation Weather Radars (CINRADs). The study domain covers an area of 600 km × 600 km (37°N–43°N, 113°E–119°E) in the Beijing–Tianjin–Hebei region (see Fig. 2).

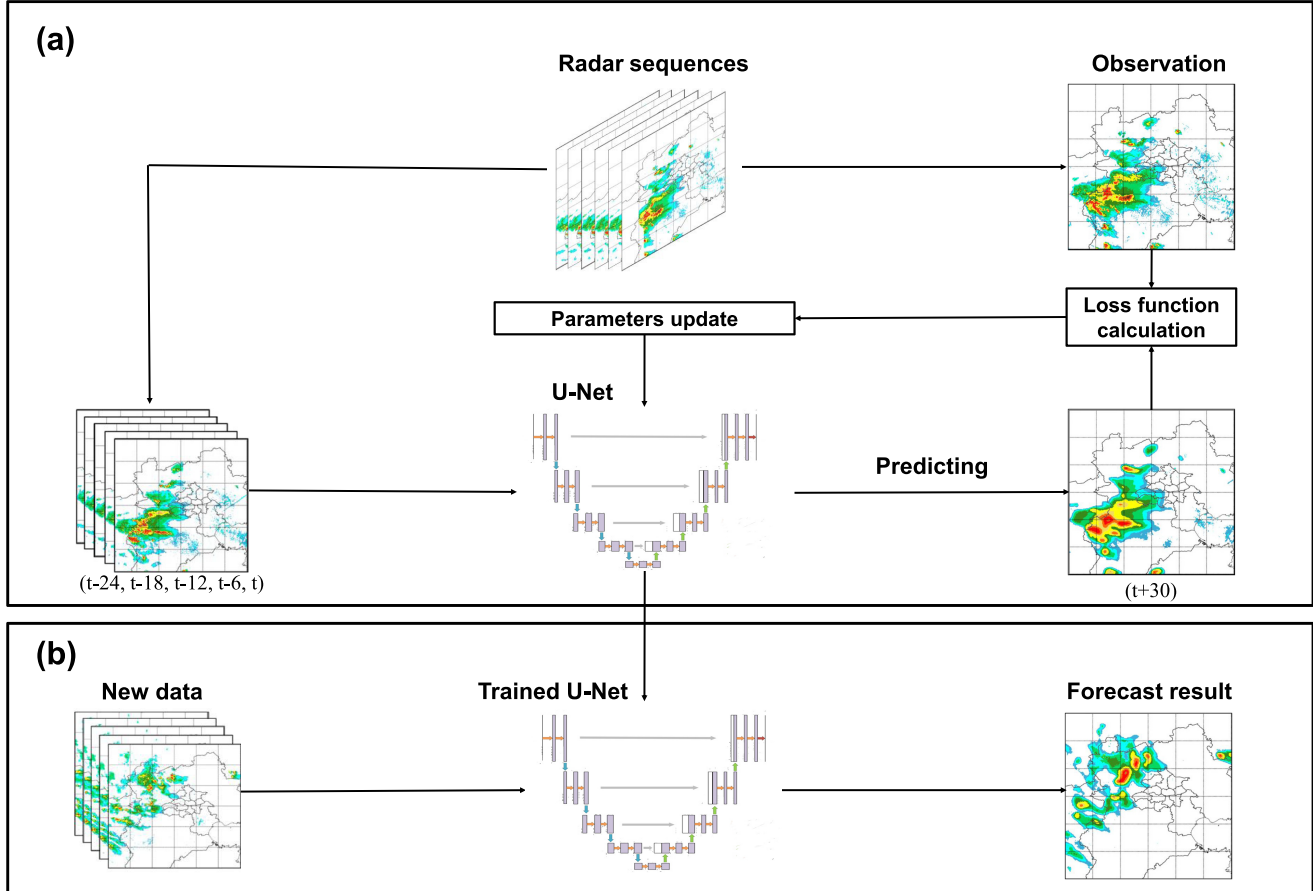


Fig. 3. Conceptual diagram of the U-Net-based radar nowcasting algorithm. (a) Training. (b) Prediction.

TABLE I
STATISTICS OF THE TRAINING, VALIDATION, AND TESTING DATASETS

	Training set	Validation set	test set
Years	2010-2016	2010-2016	2017
Days	860	62	162
Sample number	165843	12227	35531

The radar data collected during warm seasons (June to September) from 2010 to 2017 are used, which are divided into training, validation, and testing subsets. All radar reflectivity data are normalized to [0,1] by setting normalized value $\hat{Z} = (Z - \min\{Z\})/\max\{Z\} - \min\{Z\}$. In detail, 860 days of data are used as the training set, 62 days are used as the validation set to optimize the model parameters, and 162 days are used as the test set (see Table I). It should be mentioned that the training and validation sets are selected randomly from 2010 to 2016, while the 2017 data are used for testing.

IV. METHODS

Proposed first in medical image segmentation area, U-Net has achieved successes in many applications [10], [25], [26]. In this study, the nowcasting problem is first converted into an image-to-image translation problem, to which U-Net is then applied. Radar reflectivity images are used as the model

input, and the output is also radar reflectivity image. Fig. 3 presents the flowchart of the proposed algorithm. During the training period, five continuous radar reflectivity images are used as input to U-Net, and the radar reflectivity image in N min is used as the ground truth (N is set to 30 in this study). Users can select other values depending on their need. The trained U-Net is then used to make predictions on new arriving radar data. Without manual feature construction, this end-to-end method can automatically provide nowcasting in the form of radar reflectivity image based on the input radar data for the purpose of precipitation nowcasting.

A. Architecture of the Model

Fig. 4 shows the detailed architecture of our U-Net network. It has a four-layer encoder-decoder architecture [27]. The input of the model is five consecutive radar reflectivity images, and the output is N min prediction in the form of radar reflectivity image. The model includes three operations: upsampling (green arrow in Fig. 4), downsampling (blue arrow in Fig. 4), and skip connection (gray arrow in Fig. 4). The left part of the model is the encoder, which reduces the image size through convolution and max-pooling and extracts low-level features. In the encoder part, the number of filters for the CNNs is set to 16, 32, 64, and 128. The right part of the model is the decoder, which extracts high-level features and restores the output to the original size of 600×600 through layerwise upsampling

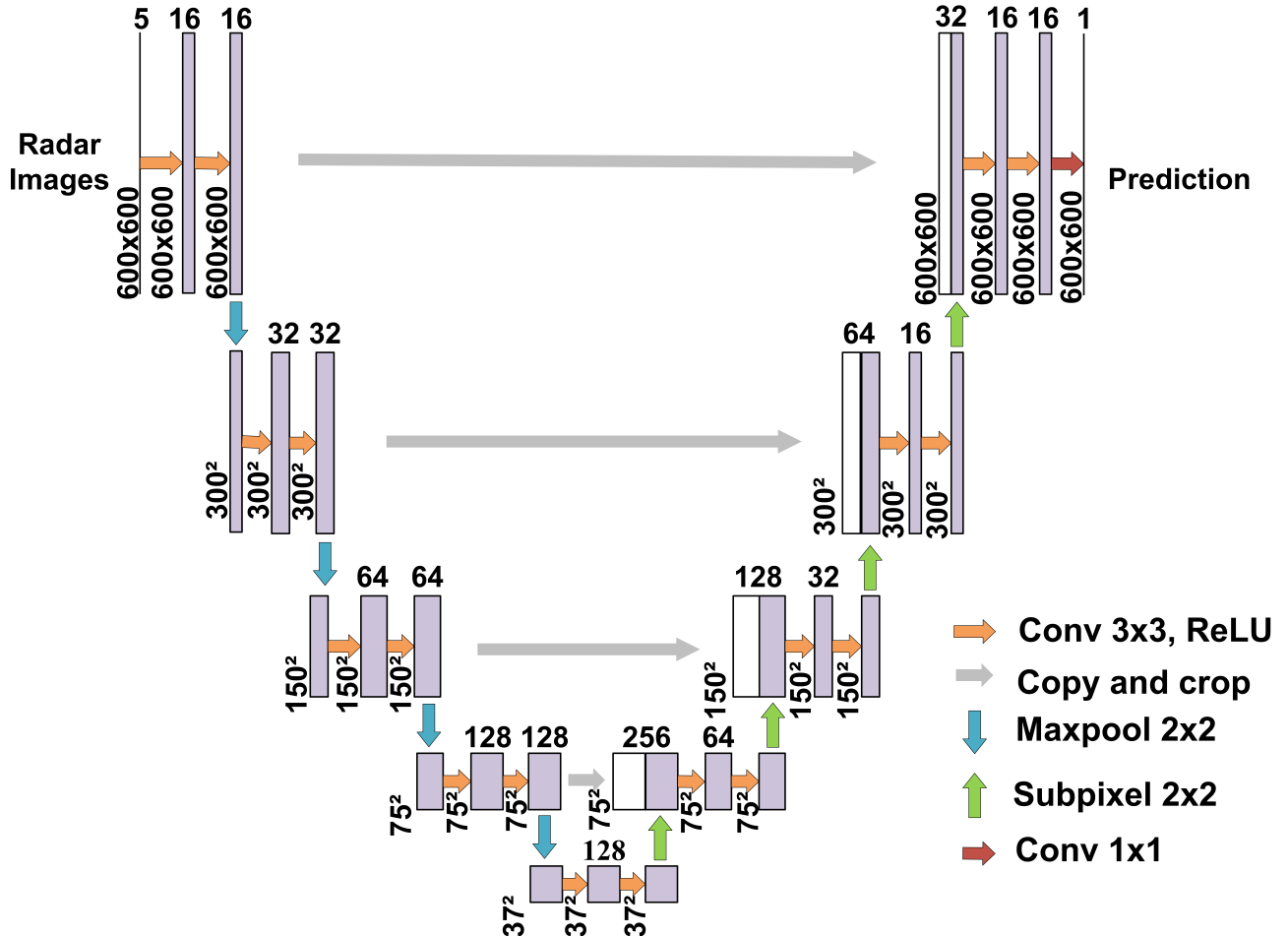


Fig. 4. Detailed architecture of the U-Net model designed for radar nowcasting.

convolutions. The bilinear interpolation [28], deconvolution [29], unpooling [30], and sub-pixel convolution are all able to accomplish the upsampling operation. The sub-pixel method is used in this study as Shi *et al.* [31] have shown that sub-pixel is superior to other methods, as the sub-pixel layer is capable of learning a better and more complex mapping filter for upsampling. For example, if a low-resolution image ($H \times W$) needs to be enlarged r times, then r^2 feature maps need to be generated by convolution. These feature maps of the same size are then stitched together to obtain an image of $rH \times rW$. The purpose of skip connections is to enable U-Net to preserve fine-scale information from shallower layers [32].

The learning rate in this study is set to 0.001. The early-stopping strategy is used for training to prevent the model from being fit too early. In addition, we use a learning rate optimization method called warmup [33]. Warmup starts training at a very small learning rate, then increases the learning rate slowly, and finally the learning rate is fixed to the set value. Adam optimizer is used in this study [34]. All experiments are conducted using PyTorch [35] and an NVIDIA 1080Ti GPU.

TABLE II
PROBABILITY DISTRIBUTION OF RADAR REFLECTIVITY
USED IN THIS STUDY

Radar Reflectivity (dBZ)	Proportion(%)
$x < 10$	90.81
$10 < x \leq 20$	5.99
$20 < x \leq 30$	2.50
$30 < x \leq 40$	0.56
$40 < x$	0.14

B. Design of Training Loss

Mean-squared error (MSE) is a traditional loss function defined as follows:

$$\text{MSE} = \frac{1}{M} \sum_{m=1}^M \sum_{i=1}^{600} \sum_{j=1}^{600} (x_{m,i,j} - \hat{x}_{m,i,j})^2 \quad (2)$$

where M is the total number of frames. $x_{m,i,j}$ and $\hat{x}_{m,i,j}$ are the observed and predicted values, respectively.

Due to extremely uneven data distribution in radar reflectivity values (see Table II), a weighted loss function is used

in this study. The weight changes with the radar reflectivity value and is designed as follows:

$$\omega(x) = \begin{cases} 1, & x < 10 \\ 2, & 10 \leq x < 20 \\ 5, & 20 \leq x < 30 \\ 10, & 30 \leq x < 40 \\ 30, & 40 \leq x \end{cases} \quad (3)$$

where x represents the radar reflectivity value. Then, the weighted loss function balanced mean-squared error (BMSE) can be computed as

$$\text{BMSE} = \frac{1}{M} \sum_{m=1}^M \sum_{i=1}^{600} \sum_{j=1}^{600} \omega_{m,i,j} (x_{m,i,j} - \hat{x}_{m,i,j})^2 \quad (4)$$

where $\omega_{m,i,j}$ is the weight of the (i, j) th pixel in the m th frame.

In addition, to pay more attention to strong radar echoes, we also add binary cross entropy loss (BCELoss) to calculate the skill score at a specific threshold $\tau = 35$ dBZ

$$\text{BCELoss} = \frac{1}{M} \sum_{m=1}^M \sum_{i=1}^{600} \sum_{j=1}^{600} -[y_{m,i,j} \log(\hat{y}_{m,i,j}) + (1 - y_{m,i,j}) \log(1 - \hat{y}_{m,i,j})]. \quad (5)$$

where $y_{m,i,j}$ and $\hat{y}_{m,i,j}$ denote the true and predicted values, respectively, of the output pixels under the condition that 35 dBZ is the threshold value. If the value is greater than 35 dBZ, the value is 1, and the opposite is 0. Another loss function considered in this study is the combination of the above two loss functions as follows:

$$\text{Loss} = \text{BMSE} + \text{BCELoss} * 0.1. \quad (6)$$

The effect of using different loss functions will be compared in Section V.

V. EXPERIMENTS AND ANALYSIS

A. Evaluating Metrics

To evaluate the performance of precipitation nowcasting, the following metrics are used: the probability of detection (POD), false alarm ratio (FAR), and critical success index (CSI) [36], [37]. The values of POD, FAR, and CSI are all between 0 and 1, where the closer the values of POD and CSI are to 1, and the closer the values of FAR are to 0, the stronger the forecasting ability of the model. POD, FAR, and CSI are defined as

$$\text{POD} = \frac{\text{TP}}{\text{TP} + \text{FN}} \quad (7a)$$

$$\text{FAR} = \frac{\text{FP}}{\text{FP} + \text{TP}} \quad (7b)$$

$$\text{CSI} = \frac{\text{TP}}{\text{TP} + \text{FP} + \text{FN}} \quad (7c)$$

where TP is the number of grid points where both the observed and predicted radar reflectivity are greater than the threshold; FP is the number of grid points where the observed reflectivity is lower than the threshold, whereas the predicted reflectivity

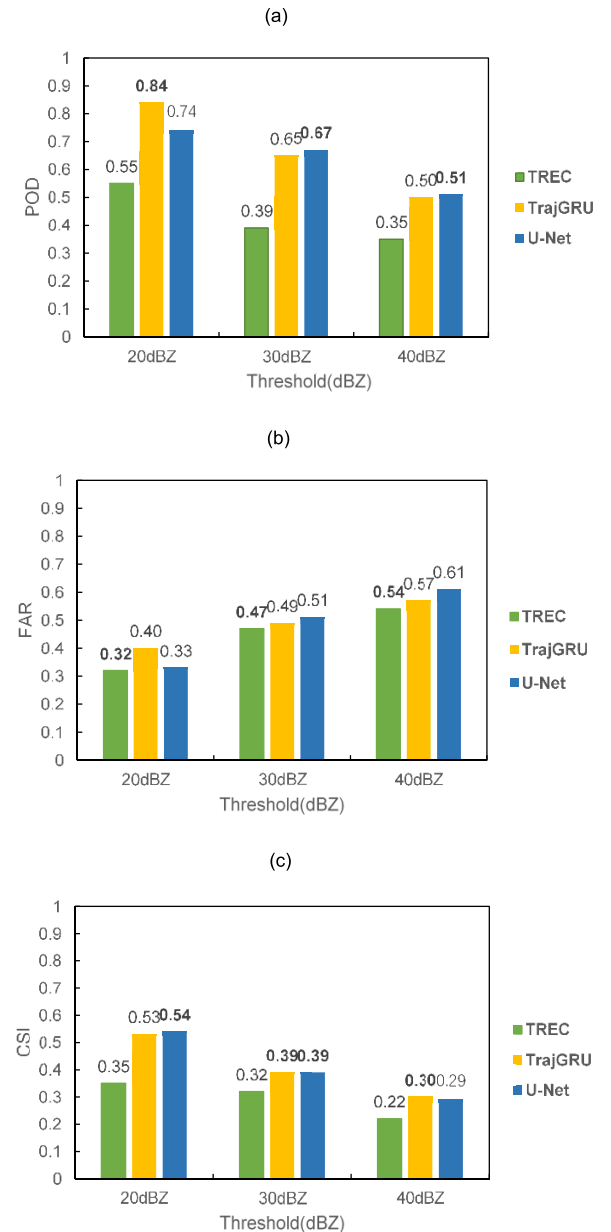


Fig. 5. Skill scores of TREC, TrajGRU, and U-Net for 30-min prediction of radar reflectivity. The best result with a specific model is marked with bold face. (a) POD. (b) FAR. (c) CSI.

is greater than the threshold; FN is the number of grid points where the observed value is greater than set threshold, whereas the predicted reflectivity is lower than the threshold.

In this study, 20, 30, 40 dBZ are used as thresholds for the propose of evaluating the method for nowcasting precipitation at different intensities. In applications, the thresholds can be easily modified according to the users' need.

B. Effect of Using Different Loss Functions

Before comparing the model prediction results, we first evaluate the effect of using different loss functions for prediction. Three loss functions are compared: MSE, BMSE, and BMSE+BCELoss. U-Net is used as the nowcasting method in this section. Table III shows the evaluation results which are given in the form of POD, FAR, and CSI.

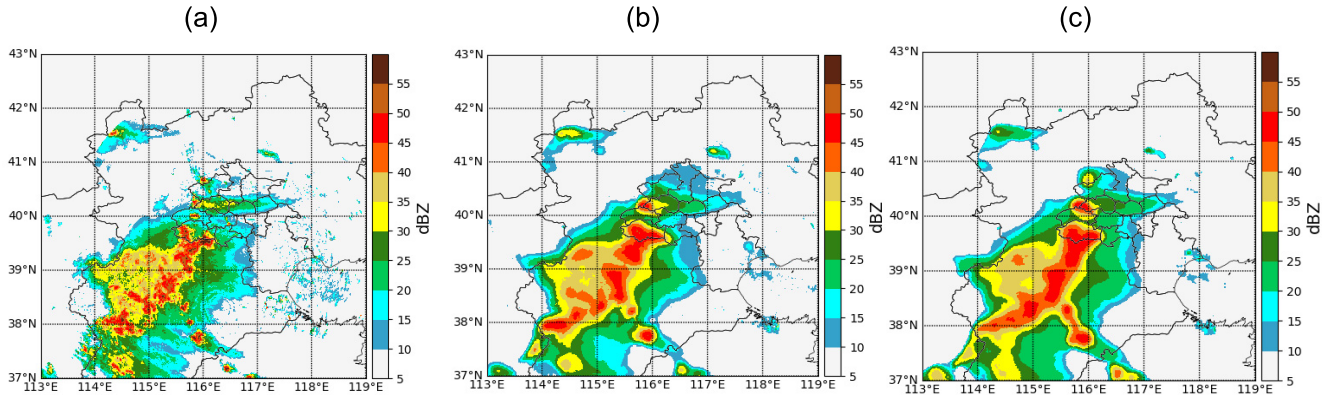


Fig. 6. Example of 30-min nowcasting results at 11:29 UTC on 21 June 2017: (a) Radar observation (truth); (b) U-Net model prediction; and (c) TrajGRU prediction.

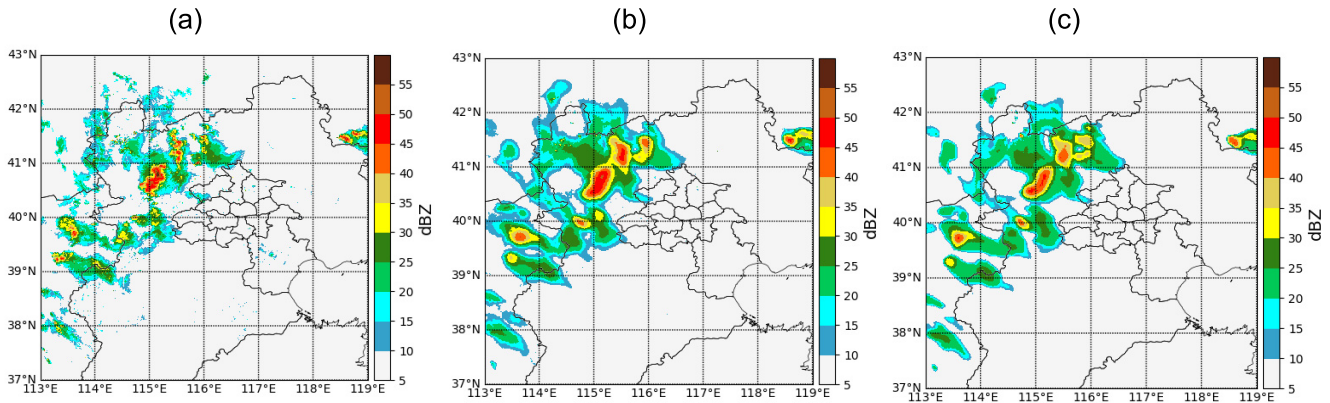


Fig. 7. Example of 30-min nowcasting results at 10:35 UTC on 31 August 2017: (a) Radar observation (truth); (b) U-Net model prediction; and (c) TrajGRU prediction.

TABLE III
SKILL SCORES OF DIFFERENT LOSS FUNCTIONS

Threshold	Loss Function	POD	FAR	CSI
20dBZ	MSE	0.65	0.22	0.55
	BMSE	0.73	0.31	0.55
	BMSE+BCELoss	0.74	0.33	0.54
30dBZ	MSE	0.49	0.34	0.39
	BMSE	0.59	0.46	0.39
	BMSE+BCELoss	0.67	0.51	0.39
40dBZ	MSE	0.24	0.39	0.20
	BMSE	0.39	0.52	0.27
	BMSE+BCELoss	0.51	0.61	0.29

The CSI values in Table III show that the BMSE+BCELoss works better than MSE and BMSE for 40 dBZ, while it has similar performance compared with other two losses for 20- and 30-dBZ thresholds. This is because, for BMSE+BCELoss, the model will focus more on strong echoes when updating parameters. This is reasonable as the convection nowcasting itself aims at strong radar echoes.

C. Results of Different Nowcasting Models

In the following, the nowcasting performances of U-Net, TREC, and TrajGRU are compared. Different from U-Net,

which is a CNN-based model, TrajGRU is a time-series model, which is good at time-series processing and has been widely used by precipitation research community. In this study, TrajGRU uses a three-layer encoding-forecasting structure with the number of filters for the RNNs set to 64, 128, and 128. The kernel size is set to 3×3 , while the number of links is 13, 13, and 9.

The experimental results are summarized in Fig. 5. Both deep learning methods outperform the TREC method, which is consistent with the results in [16]. The CNN-based U-Net can achieve almost the same performance as TrajGRU. U-Net has lower POD and FAR values for 20 dBZ, but higher POD and FAR values for 30 and 40 dBZ. As for CSI, U-Net achieves a slightly higher value than TrajGRU (0.54 versus 0.53) for 20 dBZ. Both models achieve the same CSI of 0.39 for 30 dBZ, while TrajGRU achieves a slightly higher CSI value than U-Net (0.30 versus 0.29) for 40 dBZ.

Figs. 6 and 7 present two practical examples of 30-min precipitation nowcasting. Overall, both U-Net and TrajGRU give reasonable results. As shown in the two figures, U-Net can provide more detailed inner structure in the centered big storm, which is more consistent with real observation.

VI. SUMMARY AND DISCUSSIONS

This article presents a CNN-based U-Net model for precipitation nowcasting, which contains three operations:

upsampling, downsampling, and skip connection. The symmetrical upsampling and downsampling parts form such a U-shape network architecture. In this study, three loss functions are designed. Due to extremely uneven data distribution in radar reflectivity values, the combination of a weighted loss and BCELoss is used for training. In our experiments, besides the CNN-based U-Net model, TrajGRU, which is an RNN-based model, and TREC are used for comparison. The evaluation results show that U-Net can achieve almost the same performance as TrajGRU, and both deep learning methods are superior to TREC. This result shows the great potential of CNN-based models in handling time-series applications, which can be used as a replacement of the RNN model. In future, adding an attention mechanism may help improve the accuracy of predictions.

ACKNOWLEDGMENT

The authors would like to thank NVIDIA Corporation for providing them with the Tesla GPU used in this study.

REFERENCES

- [1] J. Johnson *et al.*, “The storm cell identification and tracking algorithm: An enhanced WSR-88D algorithm,” *Weather Forecast.*, vol. 13, no. 2, pp. 263–276, 1998.
- [2] M. Dixon and G. Wiener, “TITAN: Thunderstorm identification, tracking, analysis, and nowcasting—A radar-based methodology,” *J. Atmos. Ocean. Technol.*, vol. 10, no. 6, pp. 785–797, Dec. 1993.
- [3] L. Li, W. Schmid, and J. Joss, “Nowcasting of motion and growth of precipitation with radar over a complex orography,” *J. Appl. Meteorol.*, vol. 34, no. 6, pp. 1286–1300, Jun. 1995.
- [4] R. Girshick, J. Donahue, T. Darrell, and J. Malik, “Rich feature hierarchies for accurate object detection and semantic segmentation,” in *Proc. IEEE Conf. Comput. Vis. Pattern Recognit.*, Jun. 2014, pp. 580–587.
- [5] K. He, X. Zhang, S. Ren, and J. Sun, “Spatial pyramid pooling in deep convolutional networks for visual recognition,” *IEEE Trans. Pattern Anal. Mach. Intell.*, vol. 37, no. 9, pp. 1904–1916, Sep. 2015.
- [6] R. Girshick, “Fast R-CNN,” in *Proc. IEEE Int. Conf. Comput. Vis. (ICCV)*, Dec. 2015, pp. 1440–1448.
- [7] S. Ren, K. He, R. Girshick, and J. Sun, “Faster R-CNN: Towards real-time object detection with region proposal networks,” *IEEE Trans. Pattern Anal. Mach. Intell.*, vol. 39, no. 6, pp. 1137–1149, Jun. 2017.
- [8] K. He, G. Gkioxari, P. Dollar, and R. Girshick, “Mask R-CNN,” in *Proc. IEEE Int. Conf. Comput. Vis. (ICCV)*, Oct. 2017, pp. 2961–2969.
- [9] J. Long, E. Shelhamer, and T. Darrell, “Fully convolutional networks for semantic segmentation,” in *Proc. IEEE Conf. Comput. Vis. Pattern Recognit.*, Jun. 2015, pp. 3431–3440.
- [10] O. Ronneberger, P. Fischer, and T. Brox, “U-Net: Convolutional networks for biomedical image segmentation,” in *Proc. Int. Conf. Med. Image Comput. Comput.-Assist. Intervent.*, 2015, pp. 234–241.
- [11] I. J. Goodfellow *et al.*, “Generative adversarial nets,” in *Proc. Adv. Neural Inf. Process. Syst.*, 2014, pp. 2672–2680.
- [12] M. Mirza and S. Osindero, “Conditional generative adversarial nets,” 2014, *arXiv:1411.1784*. [Online]. Available: <http://arxiv.org/abs/1411.1784>
- [13] H. Chen, V. Chandrasekar, H. Tan, and R. Cifelli, “Rainfall estimation from ground radar and TRMM precipitation radar using hybrid deep neural networks,” *Geophys. Res. Lett.*, vol. 46, nos. 17–18, pp. 10669–10678, Sep. 2019.
- [14] L. Han *et al.*, “A deep learning method for bias correction of ECMWF 24–240 h forecasts,” *Adv. Atmos. Sci.*, vol. 38, no. 9, pp. 1444–1459, Jul. 2021.
- [15] S. Xingjian, Z. Chen, H. Wang, D.-Y. Yeung, W.-K. Wong, and W.-C. Woo, “Convolutional LSTM network: A machine learning approach for precipitation nowcasting,” in *Proc. Adv. Neural Inf. Process. Syst.*, 2015, pp. 802–810.
- [16] X. Shi *et al.*, “Deep learning for precipitation nowcasting: A benchmark and a new model,” in *Proc. Adv. Neural Inf. Process. Syst.*, vol. 30, 2017, pp. 5618–5628.
- [17] Y. Wang, M. Long, J. Wang, Z. Gao, and P. S. Yu, “PredRNN: Recurrent neural networks for predictive learning using spatiotemporal LSTMs,” in *Proc. 31st Int. Conf. Neural Inf. Process. Syst.*, 2017, pp. 879–888.
- [18] Y. Wang, Z. Gao, M. Long, J. Wang, and S. Y. Philip, “PredRNN++: Towards a resolution of the deep-in-time dilemma in spatiotemporal predictive learning,” in *Proc. Int. Conf. Mach. Learn.*, 2018, pp. 5123–5132.
- [19] C. Tan, X. Feng, J. Long, and L. Geng, “FORECAST-CLSTM: A new convolutional LSTM network for cloudage nowcasting,” in *Proc. IEEE Vis. Commun. Image Process. (VCIP)*, Dec. 2018, pp. 1–4.
- [20] L. Han, Y. Zhao, H. Chen, and V. Chandrasekar, “Advancing radar nowcasting through deep transfer learning,” *IEEE Trans. Geosci. Remote Sens.*, early access, Feb. 15, 2021, doi: [10.1109/TGRS.2021.3056470](https://doi.org/10.1109/TGRS.2021.3056470)
- [21] A. Vaswani *et al.*, “Attention is all you need,” in *Proc. Adv. Neural Inf. Process. Syst.*, 2017, pp. 5998–6008.
- [22] M. Reichstein *et al.*, “Deep learning and process understanding for data-driven Earth system science,” *Nature*, vol. 566, pp. 195–204, Feb. 2019.
- [23] R. Rinehart and E. Garvey, “Three-dimensional storm motion detection by conventional weather radar,” *Nature*, vol. 273, no. 5660, pp. 287–289, 1978.
- [24] L. Han, J. Sun, and W. Zhang, “Convolutional neural network for convective storm nowcasting using 3-D Doppler weather radar data,” *IEEE Trans. Geosci. Remote Sens.*, vol. 58, no. 2, pp. 1487–1495, Feb. 2020.
- [25] P. Esser and E. Sutter, “A variational U-Net for conditional appearance and shape generation,” in *Proc. IEEE/CVF Conf. Comput. Vis. Pattern Recognit.*, Jun. 2018, pp. 8857–8866.
- [26] S. Guo, Z. Yan, K. Zhang, W. Zuo, and L. Zhang, “Toward convolutional blind denoising of real photographs,” in *Proc. IEEE/CVF Conf. Comput. Vis. Pattern Recognit. (CVPR)*, Jun. 2019, pp. 1712–1722.
- [27] I. Sutskever, O. Vinyals, and Q. V. Le, “Sequence to sequence learning with neural networks,” in *Proc. Adv. Neural Inf. Process. Syst. (NIPS)*, vol. 27, 2014, pp. 3104–3112.
- [28] E. J. Kirkland, “Bilinear interpolation,” in *Advanced Computing in Electron Microscopy*. Boston, MA, USA: Springer, 2010, pp. 261–263.
- [29] M. D. Zeiler, D. Krishnan, G. W. Taylor, and R. Fergus, “Deconvolutional networks,” in *Proc. IEEE Comput. Soc. Conf. Comput. Vis. Pattern Recognit.*, Jun. 2010, pp. 2528–2535.
- [30] M. D. Zeiler and R. Fergus, “Visualizing and understanding convolutional networks,” in *Proc. Eur. Conf. Comput. Vis.*, Sep. 2014, pp. 818–833.
- [31] W. Shi *et al.*, “Real-time single image and video super-resolution using an efficient sub-pixel convolutional neural network,” in *Proc. IEEE Conf. Comput. Vis. Pattern Recognit. (CVPR)*, Jun. 2016, pp. 1874–1883.
- [32] R. K. Srivastava, K. Greff, and J. Schmidhuber, “Training very deep networks,” in *Proc. Adv. Neural Inf. Process. Syst.*, vol. 2, Dec. 2015, pp. 2377–2385.
- [33] K. He, X. Zhang, S. Ren, and J. Sun, “Deep residual learning for image recognition,” in *Proc. IEEE Conf. Comput. Vis. Pattern Recognit. (CVPR)*, Jun. 2016, pp. 770–778.
- [34] D. P. Kingma and J. Ba, “Adam: A method for stochastic optimization,” 2014, *arXiv:1412.6980*. [Online]. Available: <http://arxiv.org/abs/1412.6980>
- [35] A. Paszke *et al.*, “Pytorch: An imperative style, high-performance deep learning library,” in *Proc. Adv. Neural Inf. Process. Syst.*, vol. 32, Vancouver, BC, Canada, Dec. 2019, pp. 8026–8037.
- [36] R. J. Donaldson, R. M. Dyer, and M. J. Kraus, “An objective evaluation of techniques for predicting severe weather events,” in *Proc. 9th Conf. Severe Local Storms, Norman, Amer. Meteorolog. Soc.*, 1975, pp. 321–326.
- [37] M. Chen, B. Bica, L. Tüchler, A. Kann, and Y. Wang, “Statistically extrapolated nowcasting of summertime precipitation over the eastern Alps,” *Adv. Atmos. Sci.*, vol. 34, no. 7, pp. 925–938, Jul. 2017.



Lei Han (Member, IEEE) received the B.Sc. degree in engineering mechanics and the M.Sc. degree in automatic control from Harbin Engineering University, Harbin, China, in 1998 and 2001, respectively, and the Ph.D. degree in atmospheric remote sensing from Beijing University of Technology, Beijing, China, in 2008.

From 2001 to 2004, he was a Software Engineer with Lucent Research and Development, Qingdao, China. From 2013 to 2014, he was a Visiting Scholar with the Earth Observation Laboratory (EOL), National Center for Atmospheric Research (NCAR), Boulder, CO, USA. He is currently an Associate Professor with the College of Information Science and Engineering, Ocean University of China, Qingdao. His research interests include radar meteorology and machine learning.



He Liang received the bachelor's degree in electronics and information engineering from Yangzhou University, Yangzhou, China, in 2018. He is currently pursuing the M.S. degree with the College of Information Science and Engineering, Ocean University of China, Qingdao, China.

His research interests include deep learning and transfer learning.



Haonan Chen (Senior Member, IEEE) received the Ph.D. degree in electrical engineering from Colorado State University (CSU), Fort Collins, CO, USA, in 2017.

He worked with the Cooperative Institute for Research in the Atmosphere (CIRA) and the NOAA Physical Sciences Laboratory, Boulder, CO, USA, from 2012 to 2020, first as a Research Student and then as a National Research Council Research Associate and a Radar, Satellite, and Precipitation Research Scientist. He is currently an Assistant

Professor with CSU. His research interests include remote sensing and multi-disciplinary data sciences, including radar and satellite observations of natural disasters, polarimetric radar systems and networking, big data analytics, multiscale hydrometeorological data fusion, and precipitation classification, estimation, and prediction using deep learning techniques.

Dr. Chen serves as an Associate Editor for the *Journal of Atmospheric and Oceanic Technology*, *URSI Radio Science Bulletin*, and the *IEEE JOURNAL OF SELECTED TOPICS IN APPLIED EARTH OBSERVATION AND REMOTE SENSING*.



Wei Zhang (Member, IEEE) received the B.S. and M.S. degrees in applied mathematics from Northeastern University of China, Shenyang, China, in 2001, and the Ph.D. degree in computer science and technology from the University of Science and Technology of China, Hefei, China, in 2004.

From 2004 to 2006, he was a Post-Doctoral Researcher with the University of Science and Technology of China. From 2013 to 2014, he was an Academic Visitor with the School of Informatics, The University of Edinburgh, Edinburgh, U.K. He is

currently an Associate Professor with the College of Information Science and Engineering, Ocean University of China, Qingdao, China. His research interests include machine learning and deep learning approaches for remote sensing and meteorology.



Yurong Ge received the bachelor's degree in electronic instruments and measuring technology from Changchun Geology College, Changchun, China, in 1994, and the Ph.D. degree in ocean information detection and processing from Ocean University of China, Qingdao, China, in 2012.

Since 1997, she has been with the College of Information Science and Engineering, Ocean University of China, where she is currently an Associate Professor. Her research interests include machine learning and deep learning approaches for remote sensing.